Earth Resistivity Estimation Based on Satellite Imaging Techniques

KWANCHAI NORSANGSRI and THANATCHAI KULWORAWANICHPONG*
Power System Research Unit
School of Electrical Engineering
Suranaree University of Technology
111 University Avenue, Nakhon Ratchasima
THAILAND
* Corresponding author, thanatchai@gmail.com

Abstract: - This paper proposes a useful technique for generating an earth resistivity map. Earth resistance is one of essential factors in a broad range of power system analysis and design. Information of earth resistivity is helpful for practical power system engineers in order to establish power system grounding. In this paper, a LANSAT7 image of a tested area of 50 km^2 was used by ENVI program in associative with a set of resistivity data obtained from field measurement. By using the maximum likelihood for supervised classification of a mixed band 7, 5 and 3, highest value of 85.71% confidence was obtained.

Key-Words: - Earth resistivity, Wenner method, Satellite image technology, Power system grounding, Classification technique, Multispectral

1 Introduction

Satellite images have found their several applications [1-5] in fields of agriculture, geology, forestry, biodiversity conservation, regional planning, education, intelligence, warfare, weather forecast, electric power system, etc. Images can be in visible colors and in other spectra. To interpret and analyze satellite images, some efficient software packages like ERDAS or ENVI are necessary. All satellite images produced by NASA are published by Earth Observatory and are freely available to the public. Several other countries, nowadays, have satellite imaging programs, and a collaborative European effort launched the ERS and Envisat satellites carrying various sensors. There are also private companies that provide commercial satellite imagery. In the early 21st century satellite imagery became widely available when affordable, easy to use software with access to satellite imagery databases became offered by several companies and organizations.

Satellite Image Technology or Remote Sensing has guided the way to the development of hyperspectral and multispectral sensors around the world as a useful tool that can be used to map specific materials by detecting specific chemical and material bonds from satellite and airborne sensors. Multispectral data obtained in space by those sensors have been exploited extensively for the past several years in a wide range of research projects such as land cover and topographic mapping, physical and biological oceanography, archaeology, etc. Research has expanded to include analysis of hyperspectral data acquired simultaneously in tens to hundreds of narrow channels. New algorithms have been developed both to exploit the spectral information of these sensors and to better deal with the computational demands of these enormous data sets. It is an excellent tool for environmental assessments, mineral mapping and land cover mapping, wildlife habitat monitoring and general land management studies. Multispectral imaging often can include large data sets and require specialized processing methods. In this paper, satellite images have been brought to estimate earth resistivity that can be used extensively in applications of power system grounding. Hyperspectral data sets of satellite images are generally composed of about 100 to 200 spectral bands of relatively narrow bandwidths (5-10 nm), whereas, multispectral data sets are usually composed of about 5 to 10 bands of relatively large bandwidths (70-400 nm). Actual detection of materials is dependent on the spectral coverage, spectral resolution, and signal-to-noise of the spectrometer, the abundance of the material and the strength of absorption features for that material in the wavelength region. In remote sensing situations, the surface materials mapped must be exposed in the optical surface and the diagnostic absorption features must be in regions of the spectrum that are reasonably transparent to the atmosphere. With these assumptions, it is possible to employ satellite images in order to visualize earth resistivity of the earth surface.

This paper consists of five main sections. Section 2 gives explanation of earth resistivity and its measurement. Section 3 covers a brief of satellite image processing. Results and discussion are put in Section 4. Section 5 presents a conclusion remark and further work.

2 Earth Resistivity and Its Measurement

Electrical equipment at all voltage levels must be earthed i.e. connected directly to an electrode driven or buried in the ground [6,7]. The resistance between the earth electrodes is critical to the safety of equipment and personnel. Usually it must be less than 100 Ω e.g. 10 Ω for an overhead line pylon. This is not always possible because of the high resistivity of some earthy materials. Earth resistivity depends on the nature of the ground, moisture content and can vary substantially. Table 1 gave information of resistivity of various soil types. Table 2 gave information of resistivity of effect of moisture content on soil resistivity. Table 3 gave information of resistivity of effect of temperature on soil resistivity. Earth resistivity, ρ_E , is a measured resistance of one unit volume of soil as shown in Fig.1. Its unit is typically assigned as ohm-meter. Also, earth resistivity can be defined by (1) in term of soil conductivity.

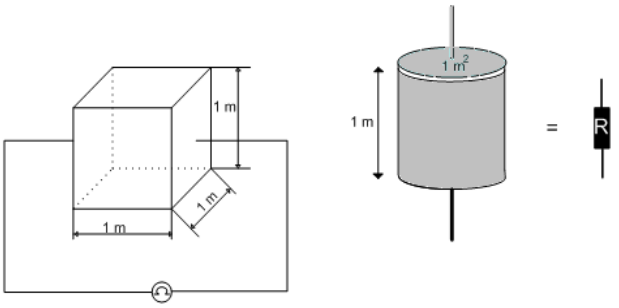

Fig. 1 Definition of earth resistivity

$$\rho = \frac{1}{\sigma} \tag{1}$$

Table 1 Resistivity of some soil materials

Materials	Resistivity (Ω·m)
Ashes	3.5
Clay soil – 40% moisture	7.7
Clay soil – 20% moisture	33
Clay – London	4-20
Clay – very dry	50-150
Chalk	50-150
Coke	0.2-8
Consolidated Sedimentary rocks	10-500
Garden earth 50% moisture	14
Garden earth 20% moisture	48
Gravel - well graded	900-1000
Gravel - poorly graded	1000-2500
Gravel clay mixture	50-400
Peat	45-200
Materials	Resistivity (Ω·m)
Sand - 90% moisture	130
Sand - normal moisture	300-800
Sand clay mixture	200-400
Surface Limestone	100-10,000

Table 2 Effect of Moisture Content on Soil Resistivity

Moisture content	Resistivity (Ω-m)		
	Top soil	Sandy loam	Red clay
2	-	1850	-
4	-	600	-
6	1350	380	-
8	900	280	-
10	600	220	-
12	350	170	1800
14	250	140	550
16	200	120	200
18	150	100	140
20	120	90	100
22	100	80	90
24	100	70	80

Table 3 Effect of Temperature on Soil Resistivity

Temperature (c°)	Resistivity (Ω-m)
-5	700
0 (ice)	300
0 (water)	100
10	80
20	70
30	60
40	50
50	40

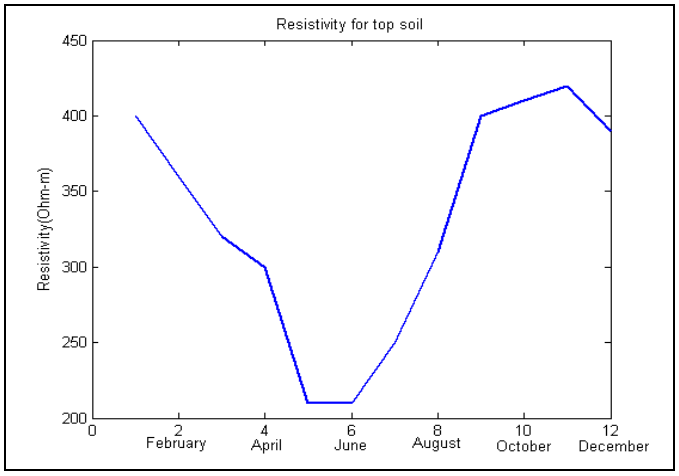

Fig. 2 Effect of Season on Resistivity

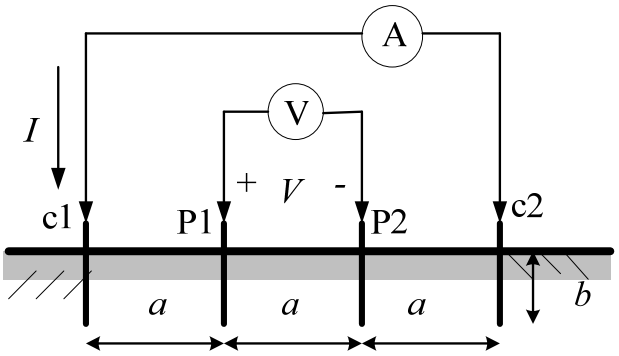

Fig. 3 Measurement of the four point method

Several methods exist to measure the earth resistance and impedance, earth resistivity and potential gradients from ground current. It is recommended that were possible the four point method (Wenner method) be used. When carrying out measurements it should be remembered that earth resistivity varies with salt contents, moisture content and temperature. Care should be taken when carrying out earth measurements as large potentials can exist between the station earth tests and remote earth's if a power system fault occurs. Four electrodes are spaced apart as shown in Fig. 3 (equally spaced or Wenner arrangement). A disadvantage of the Wenner method is the rapid decrease in potential when the spacing is increased to large values. Often commercial instruments are inadequate at measuring such low values.

According to the Wenner method, earth resistivity at the depth of *b* and the electrode spacing of *a* is given in (2) as follows.

$$\rho_E = \frac{4\pi aR}{1+\frac{2a}{\sqrt{a^2+4b^2}}-\frac{a}{\sqrt{a^2+b^2}}} \quad (2)$$

Frequently, $b < 0.05a$, (2) can be reduced to (3), where *R* denotes a measured apparent resistance.

$$\rho_E = 2\pi aR \quad (3)$$

3 Satellite Imaging Techniques

Remote Sensing is the science and art of acquiring information (spectral, spatial, temporal) about material objects, area, or phenomenon, without making any physical contact with the objects, or area, or phenomenon under investigation. Without direct contact, some means of transferring information through space must be utilized. In remote sensing, information transfer is accomplished by use of electromagnetic radiation (EMR). EMR is a form of energy that reveals its presence by the observable effects it produces when it strikes the matter. EMR is considered to span the spectrum of wavelengths from 10-10 mm to cosmic rays up to 1010 mm, the broadcast wavelengths, which extend from 0.30-15 mm.

There are two types of remote sensing, passive and active sensing techniques. Passive sensing, as described in Fig. 4, collects information about a medium based on naturally occurring signals that can be received (like the radiation emitted by an object or reflected by an object). Active remote sensing provides its own radiation and, as such, can be controlled to enable significantly more information to be gathered about the object under study as shown in Fig. 5.

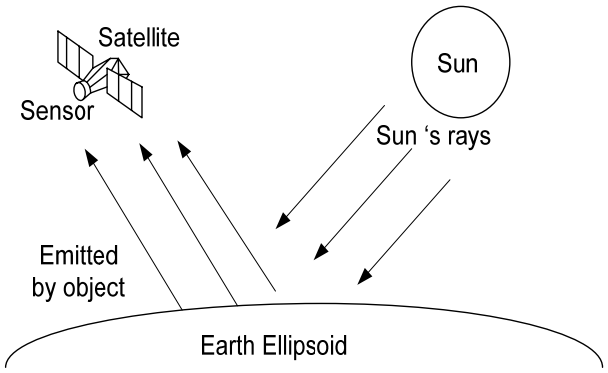

Fig. 4 Passive Remote Sensing

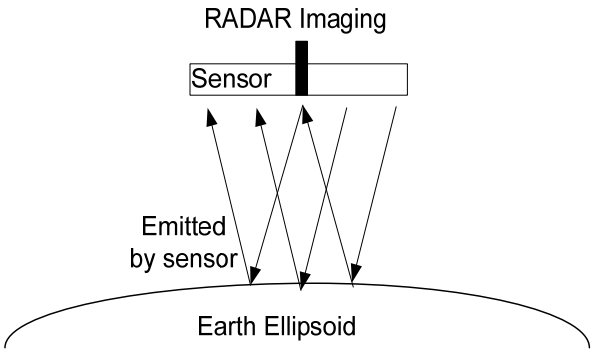

Fig. 5 Active Remote Sensing

As mentioned previously, this paper was based on aerial picture analysis. The source of these pictures came from two main sources: i) satellite images from LANDSAT and topographic map based on topographical surveys.

3.1 LANDSAT Imaging

A latest LANDSAT, LANDSAT 7, was launched in April 1999 [8]. It has a unique and essential role in the realm of earth observing satellites in orbit. The earth observing sensors on LANDSAT 7, the enhanced thematic mapper plus (ETM+), replicates the capabilities

of the thematic mapper instrument on LANDSAT 4 and 5. The ETM+ also includes new features that make it a more versatile and efficient instrument for global change studies, land cover monitoring and assessment and large area mapping. The primary new features on Landsat 7 are: i) a panchromatic band with 15m spatial resolution, ii) on board, full aperture, 5% absolute radiometric calibration and iii) a thermal IR channel with 60m spatial resolution. Fig. 6 showed a satellite image covering Thailand [9]. As mentioned earlier the dot circle is the area of study in this paper. Fig. 7 gave a close view inside the circle of Fig. 2. It revealed city of Nakhon Ratchasima from the space.

LANDSAT 7 moves around the earth with near-polar sun-synchronized orbit. It utilizes the 3.8 Giga-bits S-band communication for up- and down-link. X-band is also used for down-link purpose. Its orbital period is 16 days and time to cross the equator is 10 a.m.

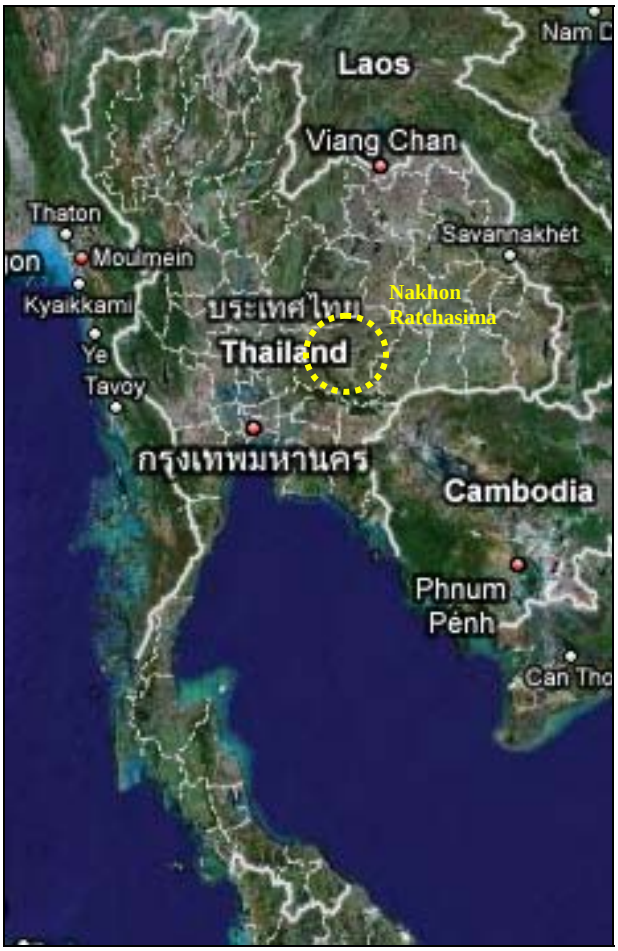

Fig. 6 Satellite image covering Thailand [9]

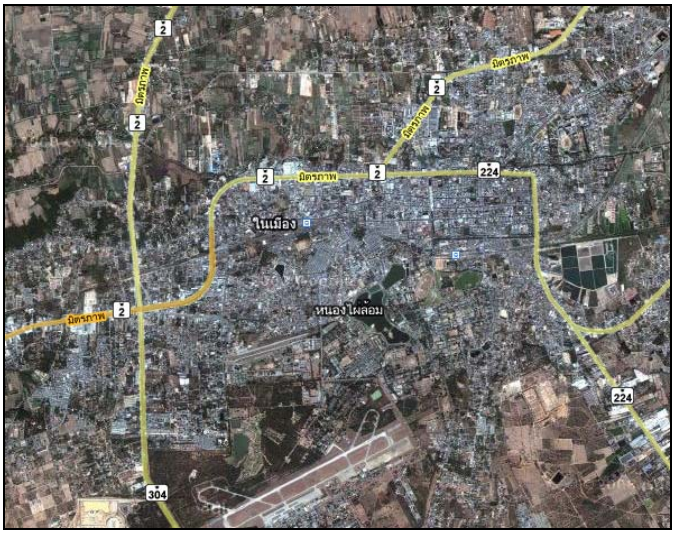

Fig. 7 Satellite image of City of Nakhon Ratchasima [8]

Satellite images acquired from LANDSAT 7 have been exploited. It depends on applications in which specific wavelengths absorbed and/or reflected from targeted materials are involved. Classification of spectral ranges of LANDSAT 7 images is given in Table 4. Fig. 8 shows coverage area of LANDSAT. However, according to applications, size of LANDSAT images is various as shown in Fig. 9. For instance, standard full scene is 183×170 km^2 per patch covering a total of 31110 km^2. It is also divided into path (P) and row (R) as imaging indices. For Nakhon Ratchasima area, P128 and R49 are codes for a LANDSAT 7 image covering that area.

Table 4 Generalized application details of spectral range

Band Number	Spectral Range (microns)	Generalized Application Details
1	0.45 - 0.52 Visible Blue	Coastal water mapping, differentiation of vegetation from soils
2	0.52 - 0.60 Visible Green	Assessment of vegetation vigour
3	0.63 - 0.69 Visible Red	Chlorophyll absorption for vegetation differentiation
4	0.76 - 0.90 Near Infrared	Biomass surveys and delineation of water bodies
5	1.55 - 1.75 Middle Infrared	Vegetation and soil moisture measurements; differentiation between snow and cloud
6	10.4 - 12.5 Thermal Infrared	Thermal mapping, soil moisture studies and plant heat stress measurement
7	2.08 - 2.35 Middle Infrared	Hydrothermal mapping, soil type, mineral
PAN	0.52 - 0.90 Green, Visible Red, Near Infrared	Large area mapping, urban change studies

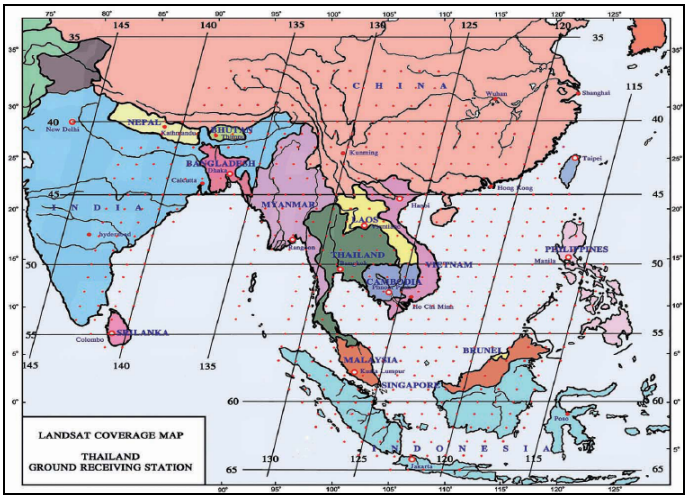

Fig. 8 LANDSAT coverage map

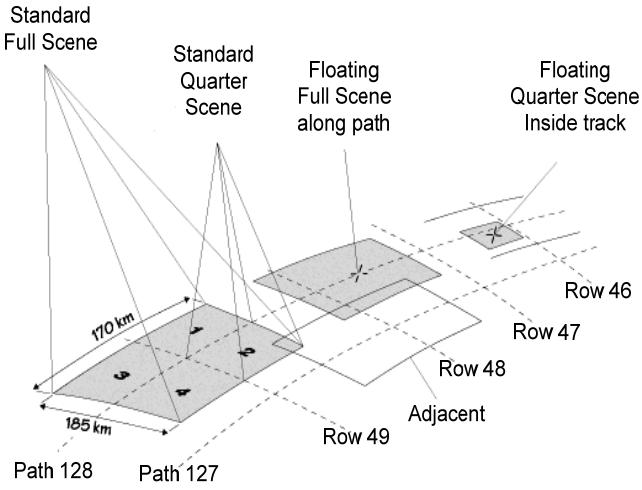

Fig. 9 Scene of satellite

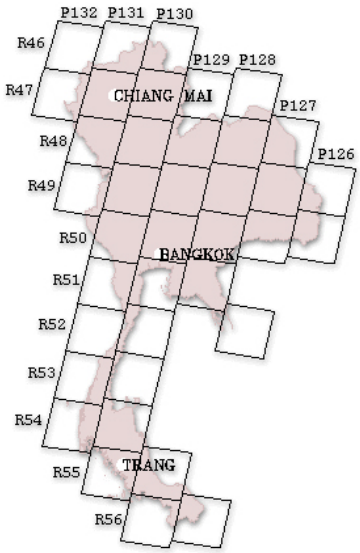

Fig. 10 Path and Row for Thailand

3.2 Classification Techniques

In order to obtained information of earth resistivity from the satellite image, two methods of classification are commonly used: unsupervised and supervised classifications [10-11]. In unsupervised classification any individual pixel is compared to each discrete cluster to see which one it is closest to. A map of all pixels in the image, classified as to which cluster each pixel is most likely to belong, is produced (in black and white or more commonly in colors assigned to each cluster). In a supervised classification the interpreter knows beforehand what classes, etc. are present and where each is in one to perhaps many locations within the scene. These are located on the image, areas containing examples of the class are circumscribed (making them training sites), and the statistical analysis is performed on the multiband data for each such class. All pixels in the image lying outside training sites are then compared with the class discriminants derived from the training sites, with each being assigned to the class it is closest to - this makes a map of established classes (with a few pixels usually remaining unknown) which can be reasonably accurate (but some classes present may not have been set up; or some pixels are misclassified.

Image classification based on maximum likelihood method is to establish groups of pixels containing similar properties as shown in Fig. 11. With the help from probability principles, any pixel can be classified into a pre-defined group that gives the distribution curve of the group closest to normal distribution. Each pixel containing information acquired from a satellite image must be assigned to be a member of the most likelihood group as described in Fig. 12. From the figure, relationship between spectral information acquired from the satellite image and earth resistivity measured from field test is featured. The weighted distance representing the likelihood can be expressed by the following relation.

$$D = \ln(a_c) - [0.5 \ln(|Cov_c|)] - [0.5(X - M_c)^T (Cov_c^{-1})(X - M_c)] \quad (4)$$

Where

D is the weighted distance (likelihood)

c is a cluster or group

X is a set of measurement vectors

M_c is a mean vector of a data group

a_c is probability of a pixel with respect to the group

Cov_c is covariance matrix of a group

$|Cov_c|$ is the determinant of Cov_c

Cov_c^{-1} = inverse matrix of Cov_c

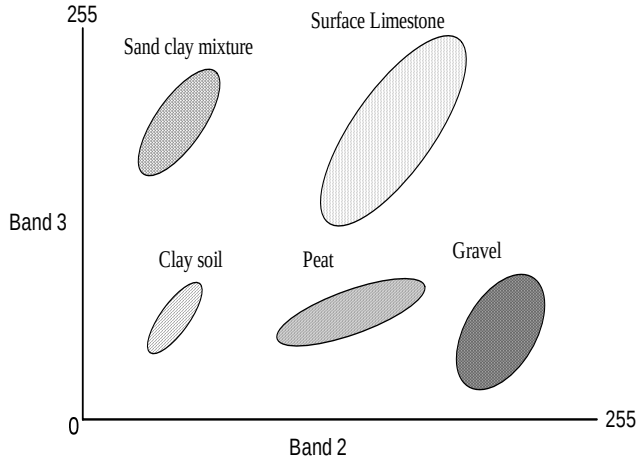

Fig. 11 Classification Techniques

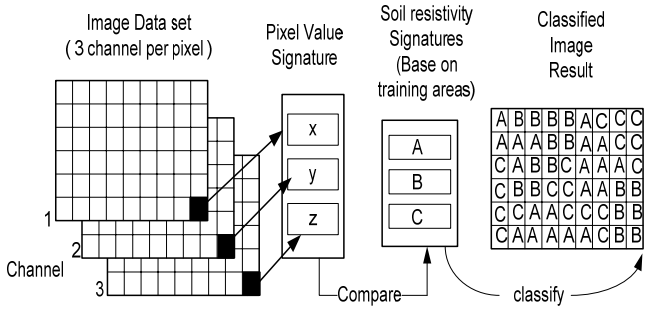

Fig. 12 Soil resistivity Classification

4 Earth Resistivity Map

4.1 Satellite Image Applications

Satellite image data is sent from the satellite to the ground station in a raw digital format, which is essentially a stream of numerical data. The smallest unit of digital data is a bit. A bit is represented by a binary number, which has only two possible values, 0 or 1. A bit can be used to represent any piece of data that has two states, such as on/off, true/false, or open/closed. With only two potential values, a bit does not offer much flexibility in representing data that is more complex than a binary number. Therefore, data is often stored as a collection of eight bits, resulting in a unit of data called a byte. It is important to remember that a satellite image is not just a picture of the target similar to what a simple camera would take. Instead it is a collection of numeric data that is capable of being displayed as an image. The underlying dataset can be manipulated using algorithms (mathematical equations) that correct for errors (like atmospheric interference), re-map the data to a geographical reference point, or extract information that is not readily apparent in the data. The data for two or more images of the same location can even be combined mathematically, creating imagery that is a composite of multiple datasets. These data products, known as derived products, can be generated by performing calculations on the raw numerical (digital numbers) data.

Classification is a process by which a set of items is grouped into classes based on common characteristics. Classification of satellite image data is based on placing pixels with similar values into groups and identifying the common characteristics of the items represented by these pixels. Classification is another tool that is very useful when multispectral imagery of the same geographical region is compared. Algorithms can be used that derive a value for each pixel in the image from its brightness values in each image. Plotting the resulting data on a 2 or 3 dimensional graph can identify clusters of pixels that share common spectral characteristics across multiple bands. This can be summarized in Fig. 13.

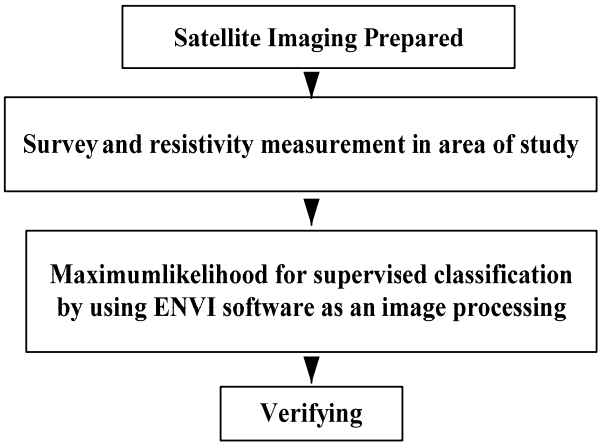

Fig. 13 Step of Classification Techniques

4.2 Satellite Imaging Prepared

A position on the Earth is referenced in the Universal Transverse Mercator (UTM) coordinate system [12] by the UTM zone, and the easting and northing coordinate pair. Each satellite image must be specified with this coordinate system. Raw satellite data often contain a vast amount of information that is not readily apparent to the analyst. Therefore, image enhancement techniques are used to highlight features of interest and expose subtle differences in the spectral signature of the components of the target. Some of these techniques involve modifying an image in order to improve contrast between features in a well defined spectral range or to improve resolution and detail, while other techniques use complex mathematical calculations to derive an entirely new image from a set of raw image data. False color [13-16] is a technique by which colors are assigned to spectral bands that do not equate to the spectral range of the selected color. This allows an analyst to highlight particular features of interest using a

color scheme that makes the features stand out. This is illustrated by Figs 14 and 15.

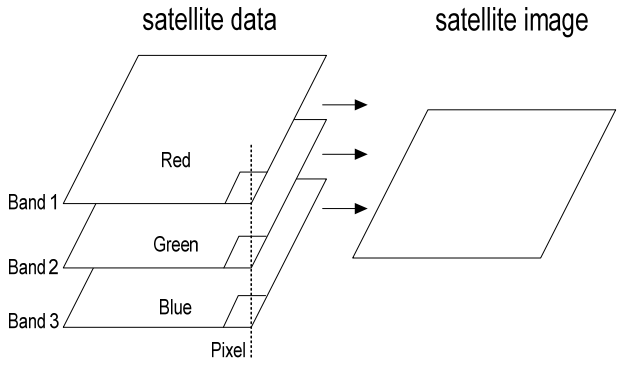

Fig. 14 Band combination for satellite images

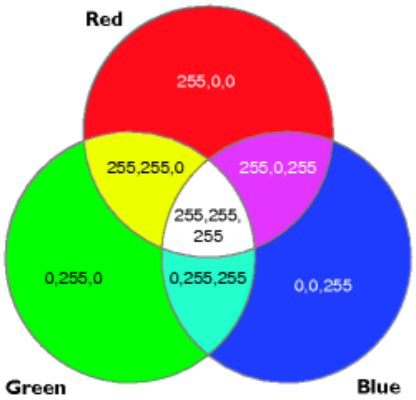

Fig. 15 Primary color: Red Green Blue

4.3 Survey and resistivity measurement in area of study

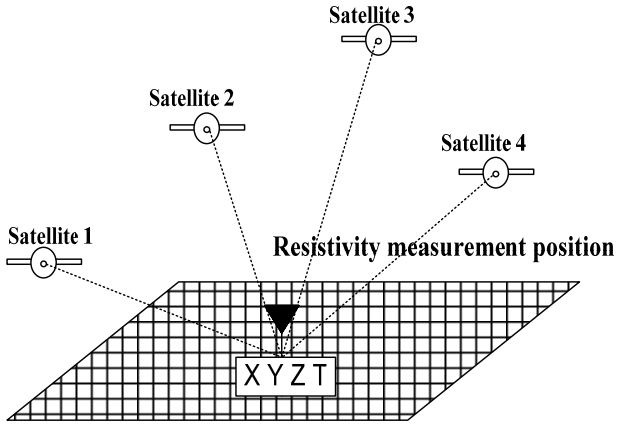

Fig. 16 GPS identification

Field measurement is necessary for supervised classification. Measured resistivity at a specific location must be determined with multispectral data of a relevant pixel. This can be performed by identifying GPS coordinate [17,18] of the test site. GPS coordinator can be used to obtain the position with respect to satellite positions as shown in Fig. 16.

4.4 Maximum likelihood for supervised classification by using ENVI software

In this paper, supervised classification based on the maximum likelihood method was employed. ENVI software was exploited as a potential tool for satellite image processing. Before performing the test, a set of data must be assigned. 50 field measurement sites were defined [19]. Then, measured values of their resistivity were obtained. 36 of all were used for classification process as shown in Table 5. Whereas, 14 left were used for accuracy assessment of the proposed method as shown in Table 6.

Table 5 Information of Survey and resistivity measurement in area of study

No	Coordinate		ρ ($\Omega.m$)	T $^{\circ}c$	RH %
1	0179439E	1646865N	6.66	33.1	11
2	0179623E	1647390N	68.9	37.2	12
3	0178534E	1648961N	12.69	33.1	9
4	0178338E	1649352N	68.2	32.3	11
5	0178874E	1649006N	70.7	31.9	12
6	0177923E	1648594N	28.1	31.9	10
7	0177770E	1647665N	38.8	32.1	8
8	0177741E	1647627N	37.2	31.1	10
9	0180230E	1645498N	34.3	31.8	12
10	0181194E	1645615N	88.3	31.5	7
11	0178568E	1647572N	50.9	35.4	10
12	0180769E	1646275N	17.95	35.1	13
13	0181344E	1645302N	505	34.0	10
14	0182339E	1645256N	1318	33.3	10
15	0184935E	1646006N	291	33.6	10
16	0183873E	1650118N	80.3	33.3	11
17	0182883E	1649397N	417	33.7	9
18	0182657E	1649214N	412	35.6	10
19	0180474E	1647819N	144.3	34.9	11
20	0179403E	1647484N	25.6	31.6	11
21	0178851E	1647829N	24.1	31.7	10
22	0178406E	1649120N	22.99	32.8	10
23	0180775E	1644079N	33.5	32.5	7
24	0183105E	1649209N	54.3	33.1	10
25	0182628E	1650235N	407	32.5	13
26	0184680E	1650178N	83.5	33.1	10
27	0183967E	1647927N	303.8	32.8	10
28	0182001E	1648069N	103.5	33.1	10
29	0180034E	1648041N	82.7	32.5	10
30	0178039E	1647984N	256.9	33.8	12
31	0177982E	1646017N	157.5	32.1	7
32	0180006E	1646017N	48.9	33.1	10
33	0181944E	1646046N	786.5	34.5	13

34	0183967E	1645989N	324.3	32.4	10
35	0184395E	1646359N	123.7	31.4	11
36	0177583E	1646929N	175.4	32.30	10

Table 6 Information of Survey and resistivity measurement in area of study for Verifying

No	Coordinate		ρ $(\Omega.m)$	T $^{\circ}c$	RH %
1	0177281E	1647068N	68.8	38.1	10
2	0178314E	1648063N	43.9	34.6	10
3	0178778E	1648388N	8.46	31.9	10
4	0179137E	1648218N	107.2	36.4	10
5	0181507E	1645293N	500	31.9	10
6	0181824E	1648579N	200	33.9	10
7	0184727E	1645344N	311	33.6	10
8	0177868E	1647043N	114.9	32.5	10
9	0181060E	1647442N	256.8	32.1	12
10	0178666E	1645390N	75.5	33.1	7
11	0178353E	1650264N	345.4	32.6	10
12	0184452E	1649067N	32.5	32.7	13
13	0179122E	1648212N	178.1	31.9	10
14	0181288E	1650634N	45.3	31.2	11

5 Results and Discussion

This research was conducted by using ENVI software as an image processing tool for extracting earth resistivity from the satellite data. A LANSAT 7 image of a tested area of 50 km^2 as shown in Fig. 17 was used for test.

Fig. 17 Satellite image of the test area

A satellite image acquired from LANSAT 7 consists of eight spectral bands with spatial resolutions ranging from 15 – 60 meters. To create earth resistivity map, five mixed bands were prepared for supervised classification as follows.

1. Bands 4-3-2
2. Bands 4-5-3
3. Bands 4-5-7
4. Bands 7-4-3
5. Bands 7-5-3

Table 7 Result of confidence level

Mixed bands	Confidence level (%)
4-3-2	64.29
4-5-3	57.14
4-5-7	71.43
7-4-3	71.43
7-5-3	85.71

50 test locations were selected and then measured for earth resistivity. 36 of all were used as input of supervised training process, while 14 left were used for verifying the effectiveness of the earth resistivity classification. Figs 18 – 22 showed visualization of five respective mixed bands as described earlier. Fig. 23-27 presented the earth resistivity map of the test area. This picture was selected from the mixed bands that gave the best estimation of the earth resistivity result. Table 7 gave results of evaluation of confidence level from the supervised classification. The results showed that the mixed bands of 7-5-3 gave the best of 85.71% confidence. The mix of bands 4-5-3 was the worst result of 57.14% confidence.

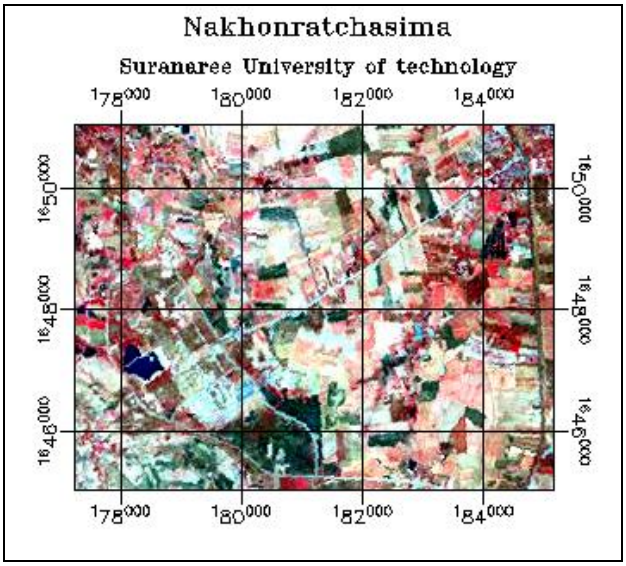

Fig. 18 Color rendering of the mixed bands 4-3-2

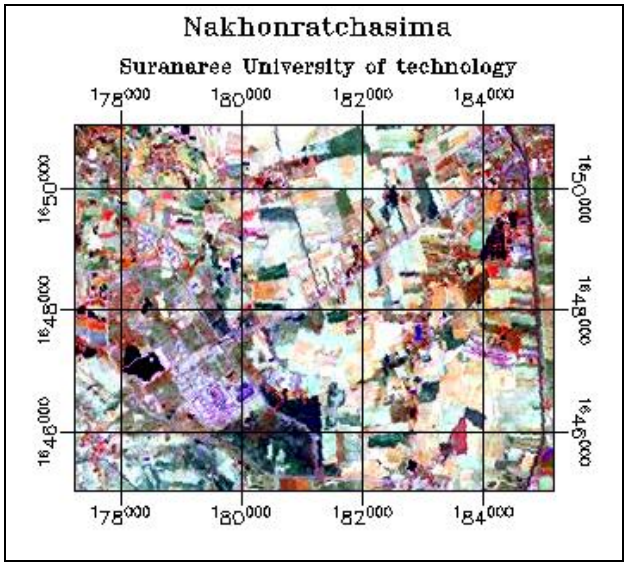

Fig. 19 Color rendering of the mixed bands 4-5-3

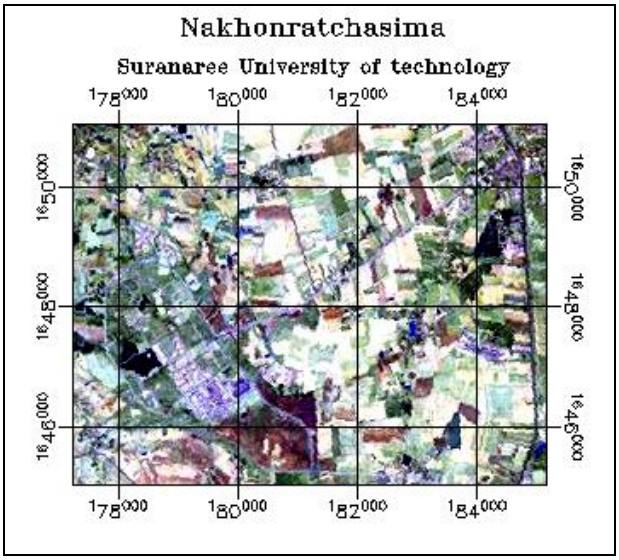

Fig. 22 Color rendering of the mixed bands 7-5-3

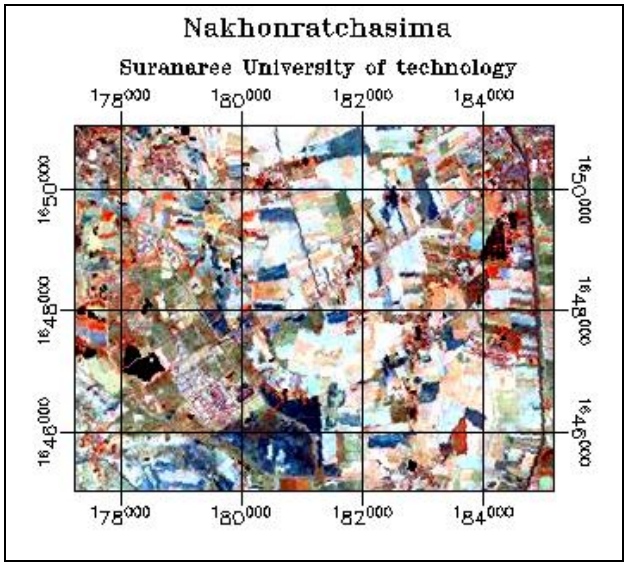

Fig. 20 Color rendering of the mixed bands 4-5-7

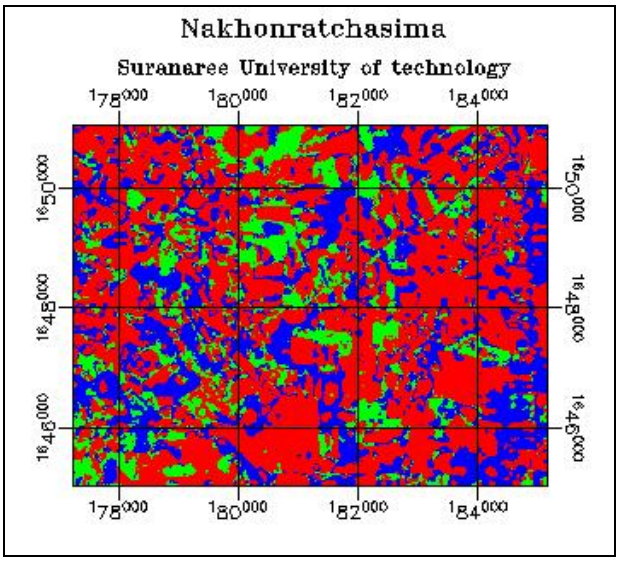

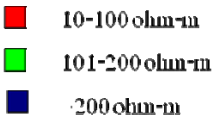

Fig. 23 Earth resistivity map of the mixed bands 4-3-2

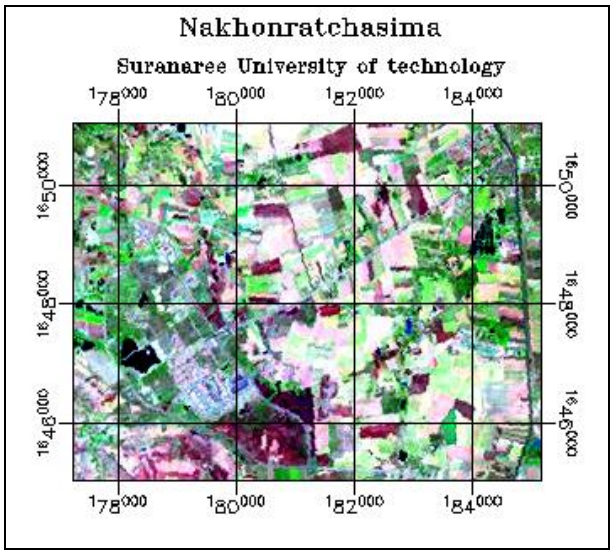

Fig. 21 Color rendering of the mixed bands 7-4-3

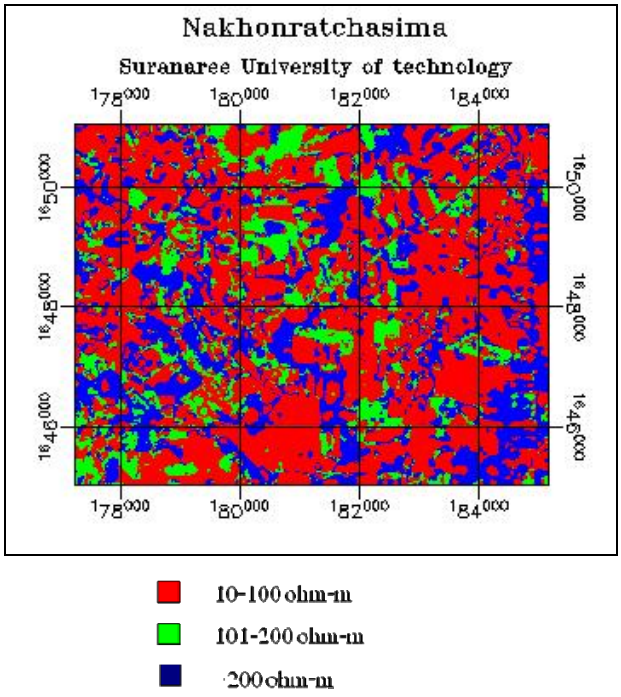

Fig. 24 Earth resistivity map of the mixed bands 4-5-3

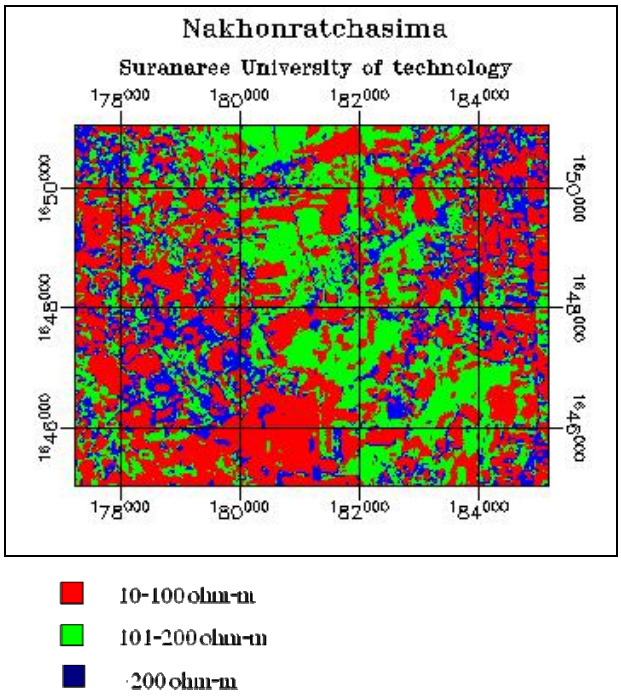

Fig. 25 Earth resistivity map of the mixed bands 4-5-7

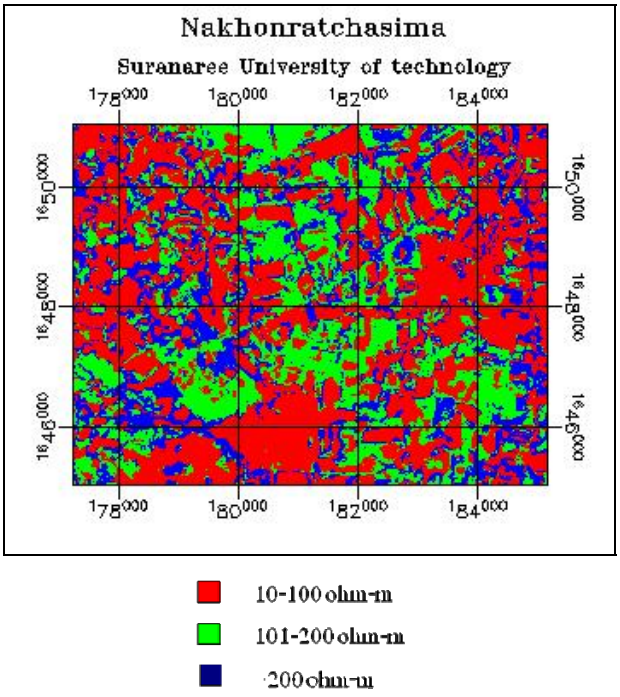

Fig. 26 Earth resistivity map of the mixed bands 7-4-3

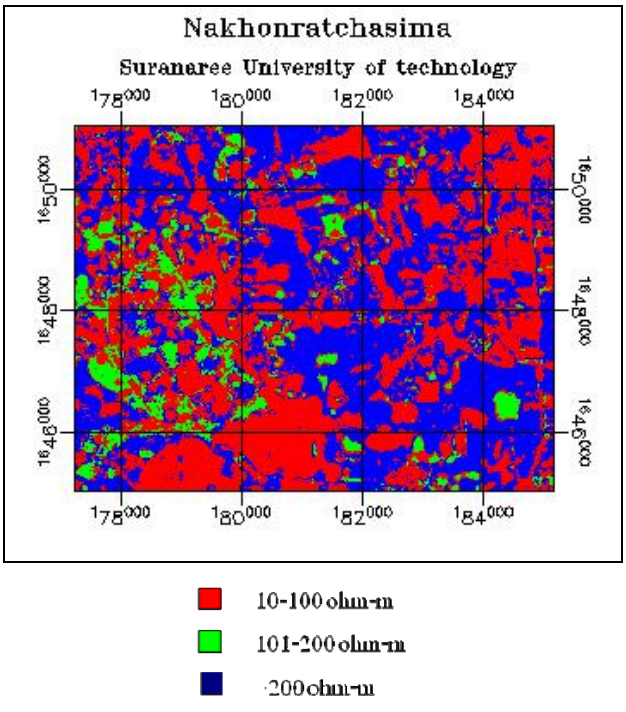

Fig. 27 Earth resistivity map of the mixed bands 7-5-3

6 Conclusion

This paper presented a satellite imaging technique of estimating earth resistivity. A 50-km^2 satellite image acquired by LANSAT 7 of the test area was used by ENVI program in associative with a set of resistivity data obtained from field measurement in order to evaluate the proposed scheme. By using the maximum

likelihood for supervised classification of a mixed band 7, 5 and 3, highest value of 85.71% confidence was obtained. The earth resistivity can be exploited in various fields, for example, power system grounding, lightning, ground fault protection, etc, in both transmission and distribution levels.

7 Acknowledgment

The authors would like to acknowledge the financial support of the research grant (E-006-51) sponsored by the Provincial Electric Authority of Thailand, during a period of this work.

References:

[1] W. Elshorbagy and A. Elhakeem, Risk assessment maps of oil spill for major desalination plants in the United Arab Emirates, *Desalination*, Volume 228, Issues 1-3, pp. 200-216, 2008

[2] X. Jin and C. H. Davis, An integrated system for automatic road mapping from high-resolution multi-spectral satellite imagery by information fusion, *Information Fusion*, Volume 6, Issue 4, pp. 257-273, 2005

[3] G. Finnveden and A. Moberg, Environmental systems analysis tools – an overview, *Journal of Cleaner Production*, Volume 13, Issue 12, pp. 1165-1173, 2005

[4] Y. Nishigami, H. Sano and T. Kojima,Estimation of forest area near deserts — production of Global Bio-Methanol from solar energy, *Applied Energy*, Volume 67, Issue 4, pp. 383-393, 2000

[5] G.P. Patil, W.L. Myers, Z. Luo, G.D. Johnson and C. Taillie, Multiscale assessment of landscapes and watersheds with synoptic multivariate spatial data in environmental and ecological statistics, *Mathematical and Computer Modelling*, Volume 32, Issues 1-2, pp. 257-272, 2000

[6] IEEE Std 142-1991,*IEEE Recommended Practice for Grounding of Industrial and Commercial Power Systems*, 1993

[7] IEEE, IEEE Guide for Measuring Earth Resistivity Ground Impedance and Earth Surface Potentials of a Ground system, 1983

[8] C. Banman, *Supervised and Unsupervised Land Use Classification*, spring session 2002

[9] http://maps.google.com/

[10] Tutorials the environment for visualizing images, ENVI version 3.2, July, 1999

[11] L. Castellana, A. D' Addabbo and G. Pasquariello, A composed supervised/unsupervised approach to improve change detection from remote sensing, *Pattern Recognition Letters*,Volume 28, Issue 4, pp.405-413, 2007

[12] N. G. Terry, Jr., How to read the Universal Transverse Mercator (UTM) Grid, *Adapted from GPS World* , pp. 32, April, 1996

[13] R.C. Gonzalez and R. E. Wood, *Digital image processing*, 3rd Edition, 2007

[14] Richards J.A., *Remote Sensing Digital Image Analysis*, Springer-Verlag, 1994

[15] H. Roosta, R. Farhudi and M.E. Afifi, Comparison between sub-pixel classifications of MODIS images: linear mixture model and neural network model, *WSEAS Trans. Environment and Development*, Issue 2, Volume 4, pp. 161 – 168, 2009

[16] T. Luemongkol, A. Wannakomol and T. Kulworawanichpong, Rerouting electric power transmission lines by using satellite imagery, *WSEAS Trans. Environment and Development*, Issue 2, Volume 5, pp. 189 – 198, 2009

[17] R. Bajaj, S. L. Ranaweera, D. P. Agrawal, GPS: Location-Tracking Technology, *Computer*, vol. 35, no. 4, pp. 92-94, Apr. 2002

[18] V. Barrile, G. Armocida and F. Di Capua, Advanced thermatic mapping: GIS/neureal networks application for tracking isoseismic lines, *WSEAS Trans. Environment and Development*, Issue 6, Volume 9, pp. 435 – 444, 2009

[19] K. Norsangsri and T. Kulworawanichpong, Application of satellite image processing to earth resistivity map, *The 9th WSEAS International Conferences on Power Systems*, 3-5 September 2009, Budapest, Hungary, pp. 137 – 141